BNL-229004-2025-JAAM

GRP-COPD-28

Electron Transfer Theory Elucidates the Hidden Role Played by Triethylamine and Triethanolamine during Photocatalysis

C. R. Carr, D. C. Grills

To be published in "Journal of the American Chemical Society"

August 2025

Chemistry Department

Brookhaven National Laboratory

U.S. Department of Energy

USDOE Office of Science (SC), Basic Energy Sciences (BES). Chemical Sciences, Geosciences & Biosciences Division (CSGB)

DISCLAIMER

Electron Transfer Theory Elucidates the Hidden Role Played by Triethylamine and Triethanolamine during Photocatalysis

Cody R. Carr,*† Michael A. Vrionides,† Ilya S. Sosulin,‡ Aliaksandra Lisouskaya,‡ Mehmed Z. Ertem,*† David C. Grills*†

†Chemistry Division, Brookhaven National Laboratory, P.O. Box 5000, Upton, New York 11973-5000, United States
‡Radiation Laboratory, University of Notre Dame, Notre Dame, Indiana, 46556, United States

Keywords: Electron transfer, pulse radiolysis, triethylamine, triethanolamine, sacrificial electron donor, photocatalysis

ABSTRACT: Triethylamine (TEA) and triethanolamine (TEOA) are renowned, in part, for their ability to reductively quench excited states by outer sphere electron transfer with vast and still growing applications as sacrificial electron donors for photocatalytic systems. Upon amine oxidation, the resulting $TEA^{\bullet+}$ and $TEOA^{\bullet+}$ radical cations undergo proton transfer (or hydrogen atom transfer), resulting in the formation of a chemical reductant that has an α-carbon centered radical adjacent to the nitrogen center ($TEA^{\bullet}$ and $TEOA^{\bullet}$). In this contribution, we have electrochemically and spectroscopically characterized a set of electron acceptors which, upon accepting an electron, are a series of photocatalysts, $[ReCl(R_1R_2\text{-bpy})(CO)_3]^{\bullet-}$, where R_1 and R_2 are electron donating and withdrawing groups in the 4,4'- and 5,5'- positions on the bipyridyl ligand. We substantiated the formation of the electron donors, $TE(O)A^{\bullet}$, by spin trapping electron paramagnetic resonance spectroscopy, where $TE(O)A^{\bullet}$ reacts with 2,4,6-tri-*tert*-butylnitrosobenzene to generate N-centered and O-centered radical adducts. Having established the chemical behaviors of the electron acceptors and donors individually, the electron transfer rate constants were determined across a 1.43 V range in driving force. The redox potential of $TEA^{\bullet}$ was benchmarked to within ±80 mV on an absolute scale in V *vs*. Fc^+/Fc in CH_3CN by using an empirical rate *vs*. free-energy correlation, electron transfer theory, and density functional theory calculations. The equilibrium potentials for $TEA^{\bullet}$ and $TEOA^{\bullet}$ were determined to be –1.98 V and –1.76 V, respectively. Based on the kinetic and thermochemical analysis presented for $TEA^{\bullet}$ and $TEOA^{\bullet}$, these transient radicals can be broadly considered strong homogeneous chemical reductants within the wider context of photoredox potentials. Thus, this work clarifies a frequently unnoticed second function for these sacrificial electron donors during photocatalysis and rationalizes the possibility of a one-photon/two-electron conversion process that is dependent on the free-energy exchange between $TE(O)A^{\bullet}$ and photocatalysts.

INTRODUCTION

In the context of photocatalysis, the most common function of a sacrificial electron donor (SED) is to reductively quench the excited state of a light-absorbing molecule, which then shuttles the excess electron either directly to a substrate or to a co-catalyst that acts *in situ* to activate the substrate. Depending on the field of research, the light absorber may be termed a photoredox catalyst or a photosensitizer. Regardless, these are molecules with suitable excited- and ground-state reduction potentials to catalytically accept and donate electrons, respectively. Rarer are self-sensitized photocatalysts, which both absorb light and catalytically transform the substrate. In any case, SEDs are deployed universally as additives within these homogeneous systems.

The tertiary amines, triethylamine (TEA) and triethanolamine (TEOA),[1] hereafter denoted collectively as TE(O)A, are widely used as SEDs in a multitude of photocatalyst systems, where they reductively quench the excited states of a variety of metal complexes.[2-8] The earliest examples utilized TEA with artificial photosystems to evolve H_2,[9] and soon thereafter TEA was leveraged in systems capable of reducing CO_2 to carbon-based products.[10] TEOA is often applied instead of TEA to serve in a more dynamic role as both a reservoir of electrons and a stabilizer of charge-separated intermediates, which in turn promotes enhanced selectivity.[10]

One-electron oxidation of TE(O)A to form the N-centered radical cation, $TE(O)A^{\bullet+}$, induces a significant increase in the acidity of the C-H bond at the adjacent α-carbon.[11] This is

the origin of the electrochemical irreversibility of the TE(O)A$^{\bullet+/0}$ couple, since TE(O)A$^{\bullet+}$ rapidly reacts with a TE(O)A molecule via proton transfer from one of its α-C–H bonds to the N-atom of TE(O)A (Scheme 1, PT pathway).[12-14] This reaction can also be described as an H-atom transfer from the α-C–H bond of TE(O)A to the N-atom of TE(O)A$^{\bullet+}$ (Scheme 1, HAT pathway).[14-16] Regardless of the pathway, TE(O)A is involved in both mechanisms to furnish one equivalent each of TE(O)AH$^+$ and the α-amino carbon-centered radical, TE(O)A$^\bullet$ (Scheme 1).

Scheme 1. Oxidation of triethylamine (TEA) causing subsequent proton transfer (PT) or hydrogen atom transfer (HAT). Equivalent reactions occur with TEOA.

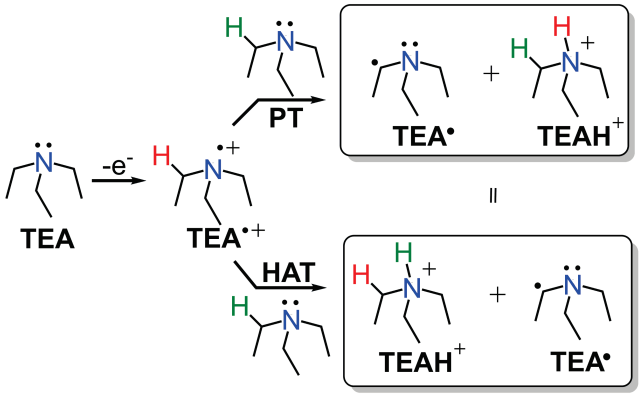

It has long been known that TE(O)A$^\bullet$ radicals are reductants, capable of reducing many photocatalysts via outer sphere electron transfer, generating iminium cations, TE(O)A$^+$, in the process (Figure 1).[13] In one classic example, the self-sensitized photocatalyst, ReCl(bpy)CO_3 (bpy = 2,2'-bipyridine), has at least two reaction pathways for reducing CO_2 to CO, dictated by the oxidation state of the metal, where TE(O)A$^\bullet$ is likely supplying an additional electron to make the faster form of the catalyst.[17, 18] Moreover, TE(O)A$^\bullet$ can influence the chemoselectivity of photoredox reactions.[5, 6] Previous contributions have deployed photochemical methods, where a short laser pulse is used to generate TE(O)A$^\bullet$, after which its one-electron oxidation is probed (Figure 1A). For example, Bhattacharyya and Das investigated the reduction of benzophenone derivatives by TEA$^\bullet$, concluding that the reduction potential of TEA$^+$, E(TEA$^{+/\bullet}$), in a 9:1 acetonitrile (CH_3CN):H_2O (v/v) mixture is between –1.9 and –2.0 V vs Fc$^{+/0}$ (Fc = ferrocene).[19] Kutal and coworkers reported that the reduction potential of TEOA$^+$ is sufficiently negative that TEOA$^\bullet$ can reduce ReBr(bpy)CO_3 in DMF ($E_{1/2}$ = –1.79 V vs Fc$^{+/0}$), and that TEA$^\bullet$ is a weaker reductant, incapable of reducing this complex under the same conditions.[7, 20, 21] Working in CH_3CN, Wayner and coworkers performed modulated photolysis to generate TEA$^\bullet$, in tandem with phase-sensitive voltammetry, to benchmark a TEA$^+$ reduction potential of –1.50 V vs Fc$^{+/0}$ in CH_3CN.[22] In contrast to Kutal's report,[20] and putting into question Wayner's TEA$^+$ reduction potential,[11, 22] our recent work in CH_3CN,[23] combining data from laser flash photolysis (Figure 1A) and pulse radiolysis (PR, Figure 1B), revealed that both TEA$^\bullet$ *and* TEOA$^\bullet$ can reduce ReCl(bpy)CO_3 in CH_3CN ($E_{1/2}$ = –1.74 V vs Fc$^{+/0}$), and that TEA$^\bullet$ is actually a more potent reductant than TEOA$^\bullet$ by ~0.2 V. However, we did not quantify the reduction potentials of TE(O)A$^+$. Thus, even though there exists a wealth of reactivity data, it is clear that the basic thermodynamic and kinetic quantities are still unknown, or at least remain ambiguous, particularly in the commonly employed solvent of CH_3CN. Therefore, the involvement of TE(O)A$^\bullet$ in photocatalytic mechanisms is often not well defined.

From this viewpoint, the current work couples the continued interest in applying TE(O)A in CH_3CN as SEDs,[2, 8, 24-29] with the grand challenge of holistically understanding photocatalytic mechanisms.[30] Until recently,[23, 31] no examples existed using PR to study catalytic mechanisms in CH_3CN, despite an enormous precedence for establishing the structure-function relationships of photocatalysts in non-aqueous solvents. In this work, through the application of PR coupled with theoretical calculations, we explore the bimolecular electron transfer reaction from TEA$^\bullet$ to a series of self-sensitized Re-based photocatalysts known for catalytic CO_2-to-CO reduction, with reduction potentials that span a range of >1.4 V (Figure 1C). In doing so, we have accurately quantified the reduction potentials of TEA$^+$ and TEOA$^+$ in CH_3CN (eq 1) through the lens of Marcus theory, and have benchmarked them versus photocatalysts in their reported catalytically active states. By this survey, the predictive power is shown to be useful for elucidating the mechanism of photocatalytic cycles involving TE(O)A by affording insight into the stoichiometric conversion of photons into electrons.

$$\text{TE(O)A}^+ + e^- \rightleftharpoons \text{TE(O)A}^\bullet \qquad E(\text{TE(O)A}^{+/\bullet}) \qquad (1)$$

RESULTS & DISCUSSION

Electrochemical Characterization of 1 – 8. Before using PR to investigate the redox reactions of TEA$^\bullet$ (Figure 1B), we first characterized the electron acceptors, S, in this system, as they serve as probe molecules to relay the dependence of the rate constant (k) on the driving force ($\Delta G°$) for electron transfer. A series of ligand-substituted, rhenium-based complexes, ReCl(R_1R_2-bpy)$(CO)_3$ (Figure 1C, bpy = 2,2'-bipyridine), previously implemented to characterize trends in catalytic activity[32, 33] and hydricity,[34] were used here to modulate changes in free energy for electron transfer. Cyclic voltammetry (CV) revealed that the first redox event for complexes **1** – **8**, denoted (**1** – **8**)$^{0/\bullet-}$, spans a range of 1.43 V (Table S1), and all are reversible, except for that of **1** (Figure 2A). The one-electron reversible redox waves produced by **2** – **8** resemble a thermodynamically-controlled (or Nernstian) process. Thus, the equilibrium potential, $E°$, was taken as the halfwave potential ($E°$= $E_{1/2}$), and the diffusion coefficients (D) were extracted from these waveforms according to the Randles–Ševčík model (Figures 2B & S1).[35] Attention was placed on the diffusion coefficients of **2** – **8** in anticipation that at least a subset of these electron acceptors may react with TEA$^\bullet$ with diffusion-limited rates. Predictably, the diffusion coefficients for **2** – **8**, Fc, and TEA (Figure S2) all scale with molar mass, as observed for a large set of small molecules in CH_3CN (Figure 2C).[36]

When deployed as a photocatalyst, the one-electron reduction of ReCl(R_1R_2-bpy)$(CO)_3$ by reductive quenching of

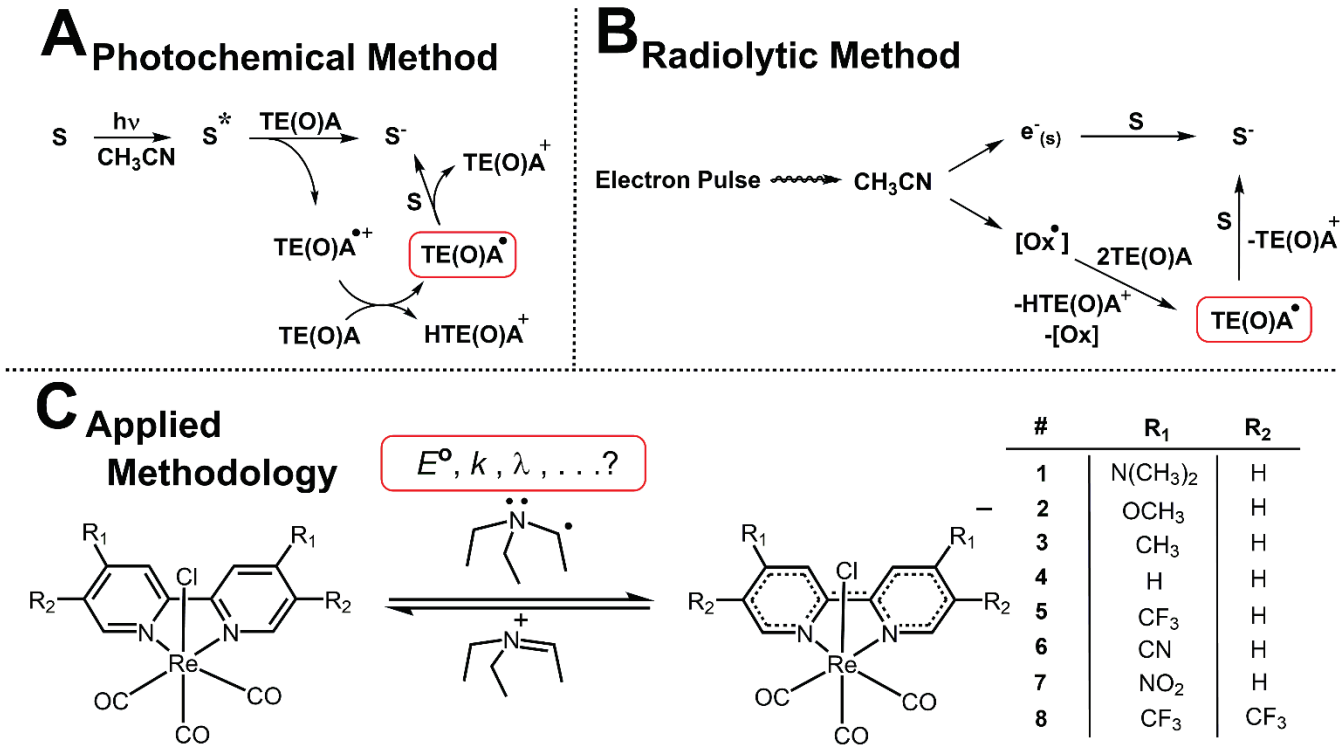

Figure 1. Developed and applied methodologies for probing the oxidation of TE(O)A• where TE(O)A notation refers to TEA and TEOA simultaneously. (**A**) Photochemical method for observing the TE(O)A• reactivity; **S**, **S**$^{-}$, and **S*** represent a generic solute in the ground state, one-electron reduced state, and excited state, respectively. (**B**) Radiolytic method for observing TE(O)A• reactivity; [Ox•] is an oxidizing radical radiolytically derived from CH_3CN solvent. (**C**) Applied radiolytic methodology to a series of $ReCl(R_1R_2\text{-bpy})CO_3$ complexes **1** – **8** used to benchmark thermal and kinetic parameters for TEA• in CH_3CN: redox potential ($E°$); bimolecular electron transfer rate constants (k); reorganization energy (λ), and structural insights gleaned from analysis.

the excited state by a sacrificial electron donor triggers dissociation of the halide ligand via charge transfer from pπ* to dz^2 (LMCT[1]), freeing a coordination site for substrate binding. The chloride ligand is typically considered fully dissociated under steady-state catalysis. However, little is known about the rate of initial chloride loss. The reversible nature of the CVs for **2** – **8** (Figure 2A), confirms that chloride dissociation from (**2** – **8**)•$^{-}$ is sufficiently slow to have no impact on the measured $E_{1/2}$. **1** is the exception because of the strongly electron donating *N,N'*-dimethylamino groups positioned at the 4,4'-postions ($\sigma_{para} = -0.83$).[37] This substituent group dramatically hastens chloride dissociation and subsequent Re–Re dimerization compared to **2** – **8**, as evident by the irreversibility of the CV and an oxidation wave at –0.9 V during the return scan, which is typical of the oxidation of $[Re(bpy)(CO)_3]_2$ dimers (Figure S3).[17, 32]

The strongly π-donating *N,N'*-dimethylamino substituent group stabilizes the empty dz^2 orbital ($LUMO^{+1}$) more than it destabilizes the occupied $dx^2\text{-}y^2$, dyz, and dxz through σ bonding (Figures 2D & S4). This enhancement in basicity of dz^2 is meaningful because the convolution created from rapid chloride dissociation coupled with electron transfer prevented a reliable $E_{1/2}$ value for **1** from being extracted from the CV data. We therefore elucidated this value by using PR[38] to measure the redox equilibrium constant.[39]

Equilibrium Redox Potential of 1 in CH_3CN. To probe the free energy of electron transfer from TEA• to **1** in CH_3CN, the equilibrium potential, $E(\mathbf{1}^{0/\bullet-})$ was determined by PR. Briefly, in the PR experiment, a short (~20 ps) energetic electron pulse (*ca.* ~9 MeV) is used to rapidly produce radical anions of solutes, whose subsequent reactivity is probed by transient absorption spectroscopy.[40, 41] Due to its high time resolution and the fact that it is not restricted to solvent systems with high conductivity or samples with any particular optical absorption profile, PR offers advantages over electrochemical and photochemical methods for the generation of reactive charge-separated intermediates. PR of CH_3CN results in the formation of the solvated electron (e^-_{solv}) as well as various solvent radicals and protons.[23, 42, 43] Since e^-_{solv} is a strong reductant and solutes are generally present in large excess, facile and rapid one-electron reduction of the solute by e^-_{solv} typically ensues as the first step. Similar to **1** (and derivatives **2** – **8**), benzophenone (BP) also rapidly scavenges e^-_{solv} in CH_3CN with a diffusion-limited rate constant (*ca.* 6.4×10^{10} M^{-1} s^{-1}), to produce the ketyl radical anion (BP•$^{-}$), with an absorption maximum at 715 nm (Figures 3A & S5). The reversible conversion of BP into BP•$^{-}$ was measured by CV at $E_{1/2}$ =–2.219 V vs. $Fc^{+/0}$ (Figure 2A, purple dotted trace). Therefore, the proximity of $E_{pc}(\mathbf{1}^{\bullet-})$ and $E_{1/2}(BP^{0/\bullet-})$, and the well-separated transient absorption bands of $\mathbf{1}^{\bullet-}$ and BP•$^{-}$, suggested that an equilibrium measurement was feasible by initially capturing e^-_{solv}.

The approach of first radiolytically generating BP•$^{-}$ from e^-_{solv} in CH_3CN, which then transfers an electron to an

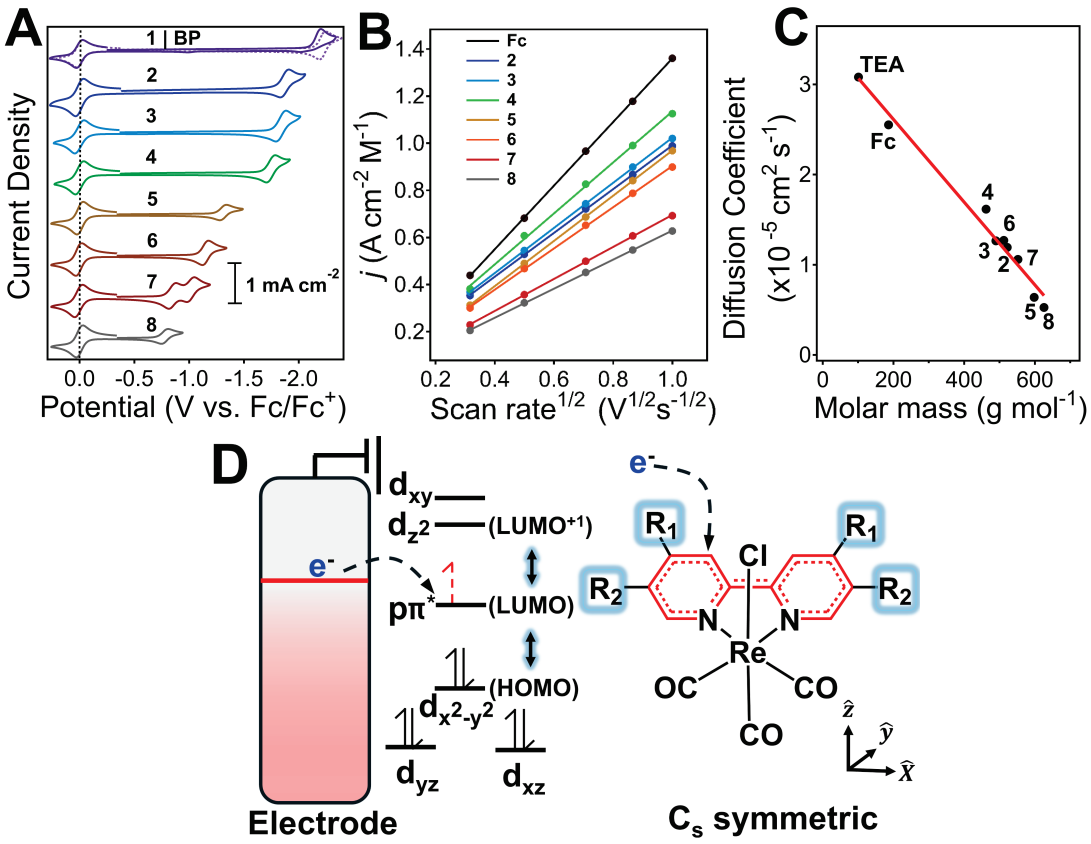

Figure 2. Electrochemical characterization of **1** – **8**. (**A**) CVs of 1 mM **1** – **8** (solid traces) and benzophenone (BP, dashed trace) in 0.1 M $TBAPF_6$ CH_3CN solution containing ferrocene (Fc, reference displayed as vertical dash) at a scan rate of 0.1 V s^{-1}. (**B**) A plot of normalized current density per molar concentration of **2** – **8** and **Fc** versus the square root of scan rate. (**C**) A plot of diffusion coefficient versus molecular weight for **2** – **8**, Fc, and TEA. (**D**) Interfacial electron transfer mechanism depicted for **1** – **8**, showing the frontier orbital energy level changes from R_1 and R_2.

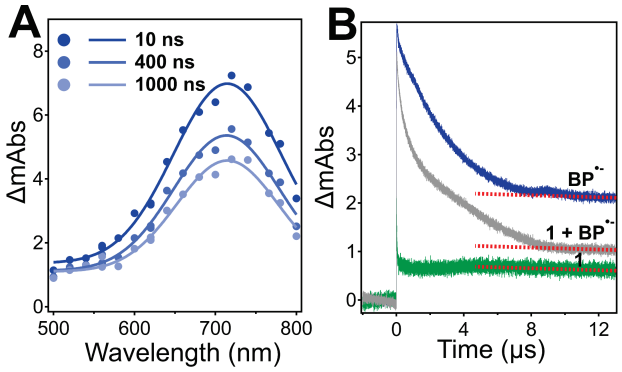

Figure 3. (**A**) UV-Vis spectra of the ketyl radical ($BP^{\bullet-}$) in 0.1 M $TBAPF_6$ CH_3CN solution (N_2-saturated) measured at the specified times after the electron pulse in a PR experiment. (**B**) Kinetic traces at λ = 720 nm from PR of N_2-saturated 0.1 M $TBAPF_6$ CH_3CN solutions containing 3.4 mM BP to observe $BP^{\bullet-}$ (blue), 0.9 mM **1** (green), and both $BP^{\bullet-}$ and **1** to observe the electron transfer equilibrium (grey).

acceptor molecule, was demonstrated by Palit and coworkers.[44] Thus, we analyzed kinetic traces at delay times after the initial decay of $BP^{\bullet-}$ (which is assigned to radical recombination processes), once an electron transfer equilibrium with **1** had been established. This is shown in Figure 3B (gray trace), where the decay trace of $BP^{\bullet-}$ in a saturated solution of **1** (*ca.* 0.9 mM, Figure S6) reached a new final amplitude compared to in the absence of **1** (blue trace), indicating that a fraction of $BP^{\bullet-}$ was oxidized by **1**. The difference between the plateau regions in the 10 to 12 μs region of the kinetic traces was used to estimate an equilibrium redox potential of –2.214 V vs. $Fc^{+/0}$ for $\mathbf{1}^{0/\bullet-}$ (see SI for detailed calculations). Constraining the redox potential to the value determined from PR in digital simulations of the CV of **1** provided a fit conducive to a reductive elimination mechanism centered at –2.214 V, which describes sequential chloride dissociation and dimerization, initiated by a single electron transfer (Scheme S1 and Figure S3). PR has been shown to have a precision of ±10 mV for the determination of the driving force of electrochemically irreversible reactions,[45] which is only slightly larger than that for $E_{1/2}$ determined electrochemically (*ca.* ±3 mV).[46] The agreement between the CV simulation and PR data lends credence to the accuracy of $E(\mathbf{1}^{0/\bullet-})$.

UV-Vis Transient Absorption Spectra of (1 – 8)$^{\bullet-}$. To establish spectroscopic handles that can be used to observe the reduction of **1** – **8** by $TEA^{\bullet}$ with transient absorption spectroscopy, the singly-reduced photocatalysts, $(\mathbf{1}-\mathbf{8})^{\bullet-}$ were generated by both UV-Vis spectroelectrochemistry (SEC) and PR. Substitution of R_1 and R_2 onto the bpy ligand

resulted in changes to the frontier orbitals in the LMCT[1] excited state (Figure 2D), generally causing a bathochromic shift of the associated absorption band on going from electron donating to withdrawing groups (Figure 4). Concentrations of **1** – **8** in the PR experiments ranged from 0.9 mM to 4.5 mM (very similar to in the CV measurements), ensuring that in all cases, the Re complexes were in large excess relative to the low micromolar-level concentrations of solvated electrons that were generated, thus maintaining pseudo-first-order kinetics for electron transfer in all cases. Confirmation that (**1** – **8**)$^{\bullet-}$ was being observed by PR was evident when (**1** – **8**)$^{\bullet-}$ was also observed within ~5 seconds of applied potential in the SEC. The spectra collected by both methods agree remarkably well (Figures 4 & S7-S8). Confidence in the assignment of **1**$^{\bullet-}$ was further enhanced by IR-SEC measurements and PR coupled with time-resolved infrared spectroscopy (PR-TRIR), the details of which can be found in the Supporting Information (See SI, "Spectral Assignment of **1**, **1**$^{\bullet-}$, and **1-CH$_3$CN**").

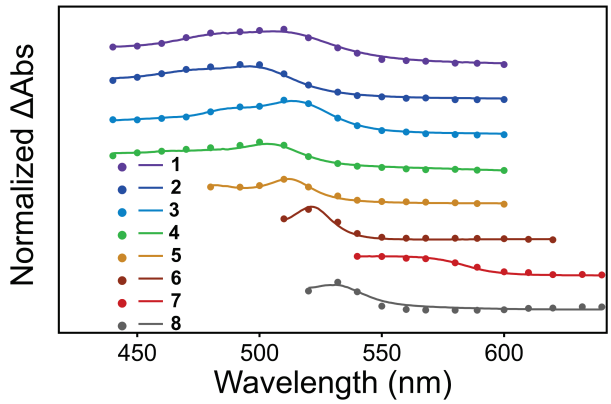

Figure 4. UV-Vis transient absorption spectra of (**1** – **8**)$^{\bullet-}$ in N_2-saturated CH_3CN, measured ~1 μs after PR (dots), overlaid with SEC spectra of solutions containing (**1** – **8**)$^{\bullet-}$ in 50 mM $TBAPF_6$ in CH_3CN after ~5 s of applied potential at the cathodic peak potential (solid lines).

Spin Trapping TE(O)A$^{\bullet}$. The α-carbon centered radicals in TE(O)A$^{\bullet}$ are prone to radical-coupling reactions as well as being a source of electrons during electron transfer. Goez and Satorius reported the structural elucidation of transient α-carbon centered amine radicals using the method of chemically induced dynamic nuclear polarization or "CIDNP".[47] It was demonstrated that the π-conjugation in triallylamine led to longer-lifetimes of its α-carbon radical compared to that of TEA$^{\bullet}$ because of the allyl *vs.* alkyl character of these radicals. McLauchlan and Ritchie used laser flash photolysis coupled with time-resolved electron paramagnetic resonance (EPR) spectroscopy to detect α-aminoalkyl radicals in solutions containing benzene-1,2:4,5-tetracarboxylic dianhydride and tertiary amines.[48] α-Aminoalkyl radicals were generated in a spin-polarized state through the triplet mechanism, enhancing their detectability by EPR. To further substantiate the formation of TE(O)A$^{\bullet}$, we deployed the photochemical method (Figure 1A) by using continuous photolysis in the presence of a photosensitizer and a spin trapping agent to measure the resulting EPR spectra under irradiation. Judiciously, BP was deployed as the photosensitizer due to its n→π* transition at 353 nm in CH_3CN (Figure S9), and negative potential of the BP$^{0/\bullet-}$ couple (Figure 2A).

To trap TE(O)A$^{\bullet}$, 2,4,6-tri-*tert*-butylnitrosobenzene (3tBNB) was used. 3tBNB reacts with primary and secondary carbon-centered radicals by addition to the nitroso (N=O) group, forming either an N–C or an O–C bond, generating a new EPR-active O-centered (N(O$^{\bullet}$)–C) or N-centered ((N$^{\bullet}$)O–C) radical spin adduct, respectively.[49] From a solution containing BP, 3tBNB, and TEA under constant visible light irradiation (>340 nm), the EPR spectrum is consistent with the formation of the (N$^{\bullet}$)O–C adduct (Figure 5B, C teal trace). In the absence of BP, the EPR spectrum revealed that 3tBNB could function as both a photosensitizer and a trapping agent during photolysis, producing the N(O$^{\bullet}$)–C adduct (Figure 5A, C purple trace). Along with the spin-adduct, a stable signal remained detectable by EPR for at least 14 min after photolysis, which can be tentatively attributed to the formation of 3tBNB$^{\bullet-}$ **,** consistent with reductive quenching of 3tBNB* by TEA (Figure S10).

The 3tBNB spin trap was also used to detect TEOA$^{\bullet}$. The EPR spectrum of a solution containing BP, 3tBNB, and TEOA during photolysis was consistent with the generation of a radical–3tBNB-adduct with a response similar to that of adducts from TEA$^{\bullet}$, albeit with significant signal broadening (Figure S11). The broadening of the spectrum is attributed to TEOA's higher viscosity compared to TEA, which constrains free rotation around single bonds in radicals, thereby masking any additional hyperfine interactions.

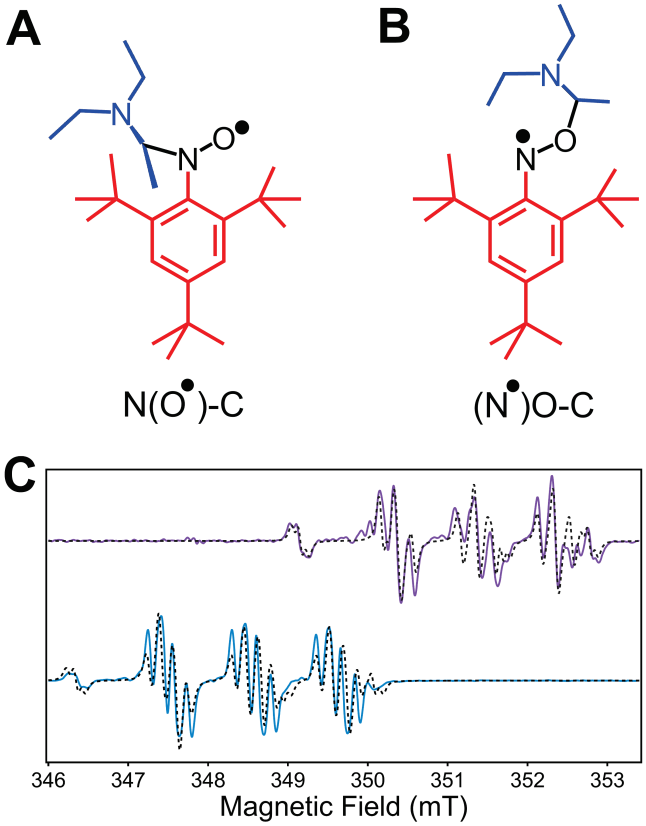

Figure 5. Structures of (**A**) N(O$^{\bullet}$)–C, and (**B**) (N$^{\bullet}$)O–C spin-trapped adducts that were detected by EPR spectroscopy

during photolysis (>340 nm) of (**C**) 300 mM BP and 2 mM 3tBNB in TEA (teal trace, (N•)O–C adduct), and 2 mM 3tBNB in TEA (purple trace, N(O•)–C adduct). The EPR spectra are normalized for clarity and simulated spectra are shown by black dashed traces (see SI for further details).

Equilibrium Redox Potentials of TEA• in CH_3CN. Having established the formation of TEA•, and the speciation, spectroscopic absorption properties, and redox potentials of the one-electron reduced photocatalysts, (**1** – **8**)•⁻ in CH_3CN solution (*vida supra*), we could then elucidate the equilibrium redox potential of TEA• by measurement of bimolecular electron transfer rate constants. This is in part by virtue of our previous work showing that TE(O)A• generation is triggered by the scavenging of radiolytically generated oxidizing solvent radicals by TE(O)A (Figure 1B), with a sub-nanosecond formation time in 1 M TE(O)A CH_3CN solution.[23] Conveniently, this is 10^3 – 10^4 times shorter than the time needed to establish equilibrium in the electron transfer reaction between TEA• and the Re catalysts, with the additional advantage that the radical scavenging provides an environment that is virtually free of reactive, oxidizing solvent radicals ([Ox•]). Whether generated photochemically or radiolytically (Figures 1A and B), the formation of **4**•⁻ was previously monitored in the mid-IR for the reduction of **4** by TEA• and TEOA•, yielding bimolecular rate constants of k = (4.4 ± 0.3) x 10^9 M^{-1} s^{-1} and (9.3 ± 0.6) x 10^7 M^{-1} s^{-1}, respectively.[23] In the current work, the same rate constant for reduction of **4** by TEA• (within a 10% margin of error) was obtained in a PR experiment that monitored the growth of **4**•⁻ by its visible absorption at 510 nm (Figure S12). Thus, visible light was subsequently used to probe the reactions of TEA• with the Re catalysts (Figures 6A and S13). Like in the PR experiments described above in the absence of TEA, the millimolar-level concentrations of the catalysts ensured pseudo-first-order kinetics for the electron transfer process with TEA•.

For 1 M TEA solutions in CH_3CN, a double-growth pattern for the formation of (**2** – **5**)•⁻ and **8**•⁻ is observed, with pseudo-first order rate constants that differ by an order of magnitude. The result is a net two-fold increase in amplitude at time delays greater than 400 ns. The reaction kinetics are showcased for **2** (Figure 6A, orange), whereby the fast component due to reduction of **2** by e^-_{solv} (green trace in Figure 6A shows this process in the absence of TEA) is separated in time from the slower component, which is due to the reduction of **2** by TEA•. We should note that the fast growth component is convoluted with the instantaneous formation of e^-_{solv} and its subsequent decay as it reacts with **2**, since e^-_{solv} also absorbs at 510 nm[42] (Figure 6A, red and blue traces show the instant growth of e^-_{solv} and its slow decay in the absence of a Re catalyst). However, this has no effect on the slower growth component. The two-component growth trend persisted in the kinetic traces for the production of (**3** – **5**)•⁻ and **8**•⁻ by e^-_{solv} and TEA•, and these data are presented in the Supporting Information (Figures S12 and S13).

The linear free-energy relationship describing the rate constants (k_{ET}) for outer-sphere electron transfer between TEA• and **2** – **4** are dependent on the driving force, $\Delta G°$, as predicted by electron transfer theory in the normal Marcus region (eq. 2). For the reactions of **5** – **8** with TEA•, the rates of electron transfer are dominated by diffusion according to the Debye–Smoluchowski model (eq. 3). The entirety of the energy surface spanning the range of driving forces for the reactions of **1** – **8** with TEA• is described as the sum of the rate constants in reciprocal space (eq. 4).[50]

$$k_{ET} = \frac{2\pi}{\hbar}|H_{ab}|^2 \frac{0.247}{\sqrt{4\pi\lambda k_b T}} e^{-\frac{(\lambda+\Delta G^0)^2}{4\lambda k_b T}} \quad (2)$$

$$k_{diff} = 4\pi r(D_a + D_d)N_a \quad (3)$$

$$\frac{1}{k} = \frac{1}{k_{ET}} + \frac{1}{k_{diff}} \quad (4)$$

In reference to Figure 6C, the fits to the energy surface were performed by constraining the redox potential of TEA• to the range, –2.03 to –1.83 V (see SI for more details) and allowing λ, $|H_{ab}|$, and k_{diff} to freely converge to minimize the least squares residuals. The rate constants for electron transfer between TEA• and **5** and **8** are diffusion-limited, i.e., $k \approx k_{diff}$ = 9.8 x 10^9 M^{-1} s^{-1}, as evident from the almost identical rate constants in the plateau region across a range of potentials. From this k_{diff} and the measured diffusion coefficients (Figure 2C), the reaction distance, r is estimated to be 3.2 Å using eq. 3. In the case of electron transfer between TEA• and **2** – **4**, the electronic coupling, reorganization energy, and free energy of the reaction are sufficiently small as to cross into a non-adiabatic and free energy-dependent regime that results in a sharp parabolic trend towards lower rate constants.[51] A reasonable assessment of the equilibrium reduction potential for TEA^+ in CH_3CN was determined as –1.98 V vs. $Fc^{+/0}$ using the Marcus theory parameters, $|H_{ab}|$ = 77 ± 22 cm^{-1} and λ = 0.8 ± 0.1 eV (see SI for further details). By initial inspection, this fit agrees well with the hypothesis that the equilibrium reduction potential of TEA^+ exists in the normal region between the $E_{1/2}$ for $\mathbf{1}^{0/•-}$ and $\mathbf{2}^{0/•-}$.[50, 52]

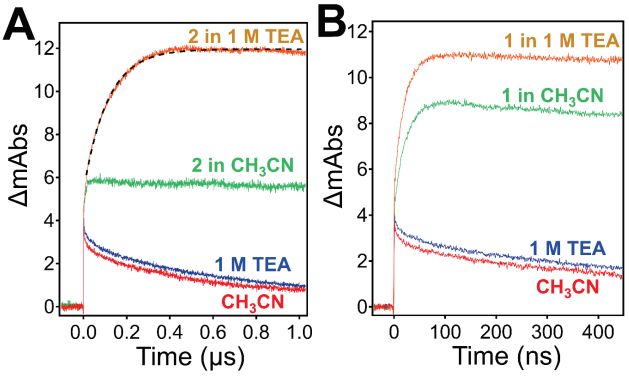

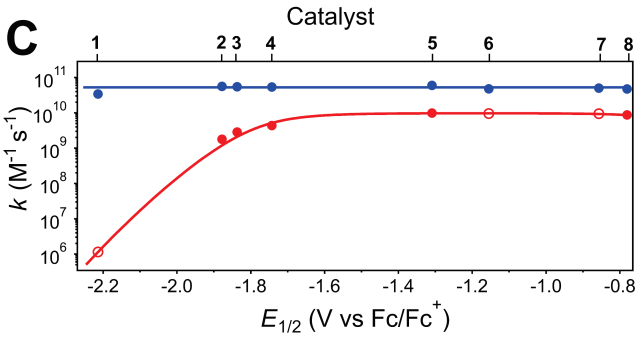

Figure 6. Mixed diffusion and electron transfer kinetics. (**A**) Growth kinetic traces of $\mathbf{2}^{\bullet-}$ measured at 510 nm after PR of a N_2-saturated CH_3CN solution containing 1 M TEA and 1.7 mM **2** (orange), with an exponential fit of the slower component shown as black dashes, and 1.7 mM **2** without TEA in CH_3CN (green). Kinetic traces are also shown in the absence of **2** with 1 M TEA (blue) and in neat CH_3CN (red). (**B**) Growth kinetic traces of $\mathbf{1}^{\bullet-}$ measured at 510 nm after PR of a N_2-saturated CH_3CN solution containing 1 M TEA and 0.9 mM **1** (orange), and 0.9 mM **1** without TEA in CH_3CN (green). Kinetic traces are also shown in the absence of **1** with 1 M TEA (blue) and in neat CH_3CN (red). (**C**) Bimolecular rate constants for electron transfer between e^-_{solv} and **2** – **8** (blue), and between TEA$^{\bullet}$ and **2** – **8** (red) versus the reduction potential, $E_{1/2}$ of **2** – **8**. Open circles designated for **1**, **6** and **7** are rate constants estimated by eqs. 2 - 4 and are not included in the fitting procedure with λ = 0.8 eV, $|H_{ab}|$ = 77 cm^{-1}, and k_{diff} = 9.8 x 10^9 M^{-1} s^{-1}; all data are summarized in Table S1.

To further support our hypothesis, the reactivity of **1** with TEA$^{\bullet}$ was investigated (Figure 6B). In the presence of 1 M TEA, while the kinetic trace for the time-resolved growth of $\mathbf{1}^{\bullet-}$ (Figure 6B, orange) also exhibits an instantaneous and a slower component, as was observed for $\mathbf{2}^{\bullet-}$ (Figure 6A), in contrast to $\mathbf{2}^{\bullet-}$, the formation of $\mathbf{1}^{\bullet-}$ is solely due to a single-step reduction of **1** by e^-_{solv}, and the fast component is simply due to the overlapping absorption of e^-_{solv} at 510 nm. This is clear from the fact that the slower growth component for $\mathbf{1}^{\bullet-}$ in Figure 6B occurs on a faster timescale than that of $\mathbf{2}^{\bullet-}$ in Figure 6A, even though the concentration of **1** was lower than that of **2**, and the reduction potential of **1** is more negative than that of **2**. Thus, the slow component cannot be due to the reduction of **1** by TEA$^{\bullet}$. However, the presence of TEA still resulted in an increase in the yield of $\mathbf{1}^{\bullet-}$ by ~20%. It is plausible that TEA mitigates the recombination of e^-_{solv} with solvent holes on picosecond time scale-+s, and/or instantaneously becomes ionized by the electron pulse.[23] [53] The net result is higher radiolytic yields of $\mathbf{1}^{\bullet-}$ (and likely for all compatible solutes) because of the increase in yield and capture of e^-_{solv} (Figure S15).

For further insight, the electron transfer driving forces for the reactions of **1** – **8** with TEA$^{\bullet}$ were computed using density functional theory (DFT) calculations at the M06-2X level of theory[54] in conjunction with the CPCM continuum solvation model[55] for CH_3CN (see SI for further details). Table 1 summarizes these results for comparison to values obtained from fits of Figure 6C using eqs. 2 – 4. Notably, the computed average of –1.98 ± 0.08 V for the TEA^+ reduction potential, and regime change from exergonic to endergonic driving forces near $\mathbf{2}^{0/\bullet-}$ are in excellent agreement with values obtained from the fitting, albeit more variations to the redox potential could be tolerated when fitting with eqs. 2 – 4. For example, variations of up to ± 0.1 V had afforded reasonable fits. In principle, this could be improved if a larger selection of catalysts with different reduction potentials were available.

Further support for the reduction potential of TEA^+ was gleaned from conducting dosimetry on solutions containing **1** (Figure S16). In saturated solution, **1** is in more than 10^3× excess compared to TEA$^{\bullet}$, leading to an inherent driving force of $-\frac{RT}{nF}\ln(\frac{[\mathbf{1}^-]}{[\mathbf{1}]})$ = 170 mV because of the initial concentration profiles after e^-_{solv} capture and before an equilibrium is established between **1** and TEA$^{\bullet}$. By this assessment, the reduction potential of TEA^+ should not be more negative than the reduction potential for $\mathbf{1}^{0/\bullet-}$ at $E_{1/2}$ +170 mV = –2.03 V. A similar analysis was conducted for the product-favored reaction between TEA$^{\bullet}$ and the free ligand from **6**, i.e., 4,4'-$(CN)_2$-2,2'-bipyridine, denoted CN-bpy. This free ligand proved useful for narrowing the range in the bracketed potential of TEA$^{\bullet}$ by ~60 mV (Figure S17). The product-favored reaction with CN-bpy implied that the potential must be more negative than $E_{1/2}$ +100 mV = –1.83 V (see SI for detailed calculation). The combined lower and upper bounded bracket potential of –2.03 and –1.83 V is consistent with –1.98 ± 0.08 V vs $Fc^{+/0}$ for $E_{TEA+/TEA\bullet}$.

Table 1. Comparison of driving forces for electron transfer from TEA$^{\bullet}$ to 1 – 8 obtained from theoretical calculations and from fits to the data in Figure 6C

Catalyst	ΔE (mV) / Theory	ΔE (mV) / Fit
1	-349	-234
2	-10	+102
3	+173	+143
4	+218	+237
5	+747	+671
6	+859	+825
7	+1076	+1123
8	+1348	+1200

In order to model the electron transfer kinetics between **1** – **8** and TEA$^{\bullet}$, we further performed theoretical calculations to estimate the reorganization energies for electron transfer at the M06-2X level of theory in addition to the driving forces (Table 1). We attempted to estimate λ values by using:

$$\lambda = \lambda_{int} + \lambda_s \qquad (5)$$

where λ_{int} accounts for the molecular structural changes and λ_s accounts for the solvent reorganization. For this purpose, geometry optimizations at the r^{2}SCAN-3c level of theory[56] in vacuum followed by single-point calculations at the M06-2X level have been performed. As a first approximation, we used the four-point scheme to calculate λ_{int} and applied the two-sphere model for λ_s (see SI for further details). Computed λ_{int} values were between 0.52 to 0.63 eV,

whereas λ_s exhibited an even narrower range of 1.01 to 1.05 eV, yielding total reorganization values of 1.54 to 1.66 eV, which are significantly higher than the λ parameter of 0.8 eV employed for the Marcus fitting. However, it should be noted that the calculated λ_s values exhibited a wide range of 0.14 to 1.09 eV depending on the estimated distance between the electron donor and acceptors in the two-sphere model (R = 4 Å and 8 Å, respectively).

Next, for the prediction of reorganization energies, we considered building model systems with explicit solvent molecules using automated molecular cluster growing approaches[56] based on the tight binding GFN2-xTB method[57] with TE(O)A$^+$ molecules as the solute. The models included 4–40 explicit solvent molecules, and we performed further geometry optimizations at the r^{2}SCAN-3c level of theory in vacuum, followed by single-point calculations at the M06-2X level in conjunction with the CPCM solvation model. We observed convergence to averaged reduction potentials for TE(O)A$^+$/TE(O)A$^\bullet$ couples over all models after inclusion of 20 explicit solvent molecules (see SI for further details). Consequently, using the models with 20 explicit solvent molecules (Figure 7), we further performed 50 ps molecular dynamics simulations and five structures were selected for the following geometry optimization and single-point energy calculation steps. Using this approach, the averaged predicted reorganization energies were 1.36 and 1.35 eV for the reaction of **4** with TEA$^\bullet$ and TEOA$^\bullet$, respectively. For this, a single model with forty solvent molecules was utilized to model only complex **4**, since it is the parent complex and the reorganization energies of the other complexes are expected to be very similar. The predicted reduction potential difference was 0.22 V for the TEA$^+$/TEA$^\bullet$ and TEOA$^+$/TEOA$^\bullet$ couples, which is in line with the experimental estimations. It should be noted that using only the CPCM continuum solvation model led to lower estimations for the λ values (1.15 and 1.04 eV for the reaction of **4** with TEA$^\bullet$ and TEOA$^\bullet$, respectively), and a similar difference in reduction potentials for the TEA$^+$/TEA$^\bullet$ and TEOA$^+$/TEOA$^\bullet$ couples (ΔE^o = 0.18 V).

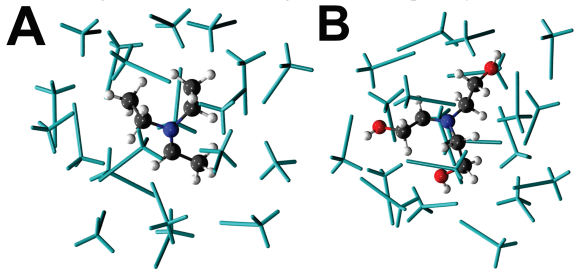

Figure 7. Structures of (**A**) TEA$^\bullet$(MeCN)$_{20}$, and (**B**) TEOA$^\bullet$(MeCN)$_{20}$ optimized at the r^2-SCAN-3c level of theory (TE(O)A$^\bullet$ as ball and stick model and solvent MeCN molecules as cyan licorice).

CONCLUSIONS

In summary, the self-sensitizing CO_2 reduction photocatalyst, **4** is reduced by TE(O)A$^\bullet$ with bimolecular rate constants that are near or at the diffusion limit. Functionalizing the bpy ligand in **4** with various electron donating and withdrawing groups created a set of electron acceptors, **1** – **8**, that were leveraged to calibrate a scale for the driving force for electron transfer with TEA$^\bullet$ over a range of 1.43 V. This Hammett approach to ligand modification resulted in minimal perturbations to diffusion behavior, reaction radius, reorganization energy, and electronic coupling, whilst maintaining adequate solubility in CH_3CN. By combining Marcus theory with computational methods, the redox potential for TEA$^\bullet$ has been benchmarked to within ±80 mV at –1.98 V vs. Fc$^{+/0}$, with that of TEOA$^\bullet$ being 0.22 V more positive, i.e., –1.76 V vs. Fc$^{+/0}$, representing substantial driving forces for electron transfer under common photocatalytic conditions when TE(O)A is typically in molar excess (*ca.* 10^3 to 10^5). The 0.8 – 1.3 eV reorganization energy measured for TEA$^\bullet$ and **4** suggests that TE(O)A$^\bullet$ can readily reduce metal-centered photosensitizers ubiquitous to many photocatalytic systems, such as [Ir(ppy)$_2$(dtbbpy)]$^+$, [Ru(bpy)$_3$]$^{2+}$, and [Ir(ppy)$_2$(phen)]$^+$, with rates that are several orders of magnitude faster than catalytic turnover frequencies. It was found that representing a scale for driving forces in a range of –1 to –2 V demonstrates the relevancy of TE(O)A$^\bullet$ towards the reduction of well-studied photocatalysts in their most reduced "catalytically active" ground states (Scheme 2). Thus, deploying TE(O)A to quench excited states in such systems also comes with a second, "hidden" fast reduction step by TE(O)A$^\bullet$ to afford a net one-photon / two-electron process depending on the relative redox potential of the electron acceptor.

Scheme 2. Half-wave potentials in V vs Fc$^{+/0}$ for TE(O)A$^\bullet$ benchmarked to selected photocatalysts in catalytically active reduced states that have been applied in CH_3CN solution with TE(O)A. [4, 5, 24, 27, 58-60]

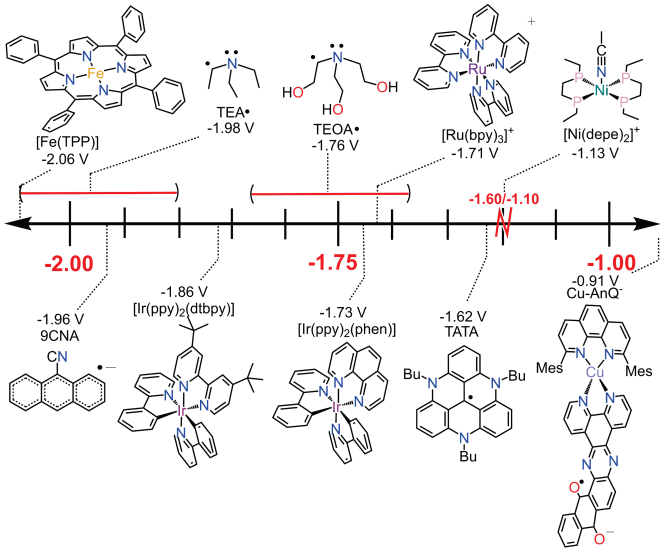

ASSOCIATED CONTENT

This supporting information is available free of charge at http://pubs.acs.org.

Detailed experimental procedures, calculations, ^{1}H-NMR spectra, characterizations of the catalysts, additional kinetic traces at different concentrations, and calculations made from DFT-

optimized structure. The data that support the findings of this study are openly available in Zenodo at https://doi.org/10.5281/zenodo.15497166

AUTHOR INFORMATION

Corresponding Authors

Cody R. Carr - *Chemistry Division - Brookhaven National Laboratory, P.O. Box 5000, Upton, New York 11973-5000, United States ; https://orcid.org/0000-0003-4166-2855*
Email: crcarr@bnl.gov

Mehmed Z. Ertem - *Chemistry Division - Brookhaven National Laboratory, P.O. Box 5000, Upton, New York 11973-5000, United States ; https://orcid.org/0000-0003-1994-9024*
Email: mzertem@bnl.gov

David C. Grills - *Chemistry Division - Brookhaven National Laboratory, P.O. Box 5000, Upton, New York 11973-5000, United States ; https://orcid.org/0000-0001-8349-9158*
Email: dcgrills@bnl.gov

Author Contributions

All authors have given approval to the final version of the manuscript.

Notes

The authors declare no competing financial interest.

ACKNOWLEDGMENT

This work and use of the Laser Electron Accelerator Facility of the Accelerator Center for Energy Research at BNL, was supported by the U.S. Department of Energy (DOE), Office of Science, Office of Basic Energy Sciences, Division of Chemical Sciences, Geosciences & Biosciences under contract DE-SC0012704. Theoretical calculations were performed utilizing computational resources at the Center for Functional Nanomaterials, which is a U.S. Department of Energy Office of Science Facility, and the Scientific Data and Computing Center, a component of the Computational Science Initiative, at Brookhaven National Laboratory under Contract No. DE-SC0012704. M. A. V. is grateful to the DOE and BNL's Office of Educational Programs for a SULI internship. The EPR spectroscopy experiments at the Notre Dame Radiation Laboratory were supported by the U.S. Department of Energy, Office of Science, Office of Basic Energy Sciences, under Award Number DE-FC02-04ER15533;document number NDRL-5468. We thank Drs. John Miller and Mathew Bird for their insightful discussions about electron transfer theory.

ABBREVIATIONS

TEA•	Triethylamine
TEOA•	Triethanolamine
SED	Sacrificial electron donor
HAT	Hydrogen atom transfer
PT	Proton transfer
ET	Electron transfer
3tBNB	2,4,6-tri-*tert*-butylnitrosobenzene
bpy	2,2'-bipyridine
BP	Benzophenone
CN-bpy	4,4'-dicyano-2,2'-bipyridine
phen	1,10-phenanthroline
ppy	2-phenylpyridine
dtbbpy	4,4'-di-*tert*-butyl-2,2'-bipyridine
Fc	Ferrocene
S	Solute
S-	One-electron reduced state of solute
S*	Excited state of solute
[Ox•]	Oxidizing radical
$\Delta G°$	Standard free energy
$E°$	Standard redox potential
$E_{1/2}$	Halfwave potential
D	Diffusion coefficient
k	Bimolecular rate constant
k_{ET}	Electron transfer rate constant
k_{diff}	Diffusion rate constant
λ	Reorganization energy
$\lvert H_{ab}\rvert$	Coupling constant
ν_{CO}	Carbonyl vibrational energy
k_b	Boltzmann's constant
T	Temperature in Kelvin
r	Reaction radius
R	Gas constant
σ_{para}	Hammett parameter
N_a	Avogadro's number
V	Volts versus ferrocene
F	Faraday's constant
n	Number of electrons
PR	Pulse radiolysis
CV(s)	Cyclic voltammetry/voltammogram(s)
EPR	Electron Paramagnetic Resonance

REFERENCES

(1) Roose, P.; Eller, K.; Henkes, E.; Rossbacher, R.; Höke, H. Amines, Aliphatic. In *Ullmann's Encyclopedia of Industrial Chemistry*, 2000; pp 1-55.

(2) Pellegrin, Y.; Odobel, F. Sacrificial electron donor reagents for solar fuel production. *C. r., Chim.* **2017**, *20* (3), 283-295. DOI: 10.1016/j.crci.2015.11.026.

(3) Kalyanasundaram, K. Photophysics, photochemistry and solar energy conversion with tris(bipyridyl)ruthenium(II) and its analogues. *Coord. Chem. Rev.* **1982**, *46*, 159-244. DOI: 10.1016/0010-8545(82)85003-0.

(4) Prier, C. K.; Rankic, D. A.; MacMillan, D. W. C. Visible Light Photoredox Catalysis with Transition Metal Complexes: Applications in Organic Synthesis. *Chem. Rev.* **2013**, *113* (7), 5322-5363. DOI: 10.1021/cr300503r.

(5) Draper, F.; Doeven, E. H.; Adcock, J. L.; Francis, P. S.; Connell, T. U. Extending Photocatalyst Activity through Choice of Electron Donor. *J. Org. Chem.* **2023**, *88* (10), 6445-6453. DOI: 10.1021/acs.joc.2c02460.

(6) Connell, T. U.; Fraser, C. L.; Czyz, M. L.; Smith, Z. M.; Hayne, D. J.; Doeven, E. H.; Agugiaro, J.; Wilson, D. J. D.; Adcock, J. L.; Scully, A. D.; et al. The Tandem Photoredox Catalysis Mechanism of $[Ir(ppy)_2(dtb\text{-}bpy)]^+$ Enabling Access to Energy Demanding Organic Substrates. *J. Am. Chem. Soc.* **2019**, *141* (44), 17646-17658. DOI: 10.1021/jacs.9b07370.

(7) Aranzaes, J. R.; Daniel, M.-C.; Astruc, D. Metallocenes as references for the determination of redox potentials by cyclic voltammetry Permethylated iron and cobalt sandwich complexes, inhibition by polyamine dendrimers, and the role of hydroxy-containing ferrocenes. *Can. J. Chem.* **2006**, *84* (2), 288-299. DOI: 10.1139/v05-262.

(8) Takeda, H.; Cometto, C.; Ishitani, O.; Robert, M. Electrons, Photons, Protons and Earth-Abundant Metal Complexes for

Molecular Catalysis of CO_2 Reduction. *ACS Catal.* **2017**, *7* (1), 70-88. DOI: 10.1021/acscatal.6b02181.

(9) Bolton, J. R.; Hall, D. O. Photochemical conversion and storage of solar energy. *Annu. Rev. Energy* **1979**, *4* (1), 353-401.

(10) Lehn, J.-M.; Ziessel, R. Photochemical generation of carbon monoxide and hydrogen by reduction of carbon dioxide and water under visible light irradiation. *PNAS* **1982**, *79* (2), 701-704.

(11) Wayner, D. D. M.; Dannenberg, J. J.; Griller, D. Oxidation potentials of α-aminoalkyl radicals: bond dissociation energies for related radical cations. *Chem. Phys. Lett.* **1986**, *131* (3), 189-191. DOI: 10.1016/0009-2614(86)80542-5.

(12) Portis, L. C.; Bhat, V.; Mann, C. K. Electrochemical dealkylation of aliphatic tertiary and secondary amines. *J. Org. Chem.* **1970**, *35* (7), 2175-2178.

(13) Whitten, D. G. Photoinduced electron transfer reactions of metal complexes in solution. *Acc. Chem. Res* **1980**, *13* (3), 83-90.

(14) Hu, J.; Wang, J.; Nguyen, T. H.; Zheng, N. The chemistry of amine radical cations produced by visible light photoredox catalysis. *Beilstein J. Org. Chem* **2013**, *9* (1), 1977-2001. DOI: 10.3762/bjoc.9.234.

(15) Chan, S.-F.; Chou, M.; Creutz, C.; Matsubara, T.; Sutin, N. Mechanism of the formation of dihydrogen from the photoinduced reactions of poly(pyridine) ruthenium(II) and poly(pyridine) rhodium(III) complexes. *J. Am. Chem. Soc.* **1981**, *103* (2), 369-379.

(16) DeLaive, P. J.; Sullivan, B.; Meyer, T.; Whitten, D. Applications of light-induced electron-transfer reactions. Coupling of hydrogen generation with photoreduction of ruthenium (II) complexes by triethylamine. *J. Am. Chem. Soc.* **1979**, *101* (14), 4007-4008.

(17) Hayashi, Y.; Kita, S.; Brunschwig, B. S.; Fujita, E. Involvement of a Binuclear Species with the Re−C(O)O−Re Moiety in CO_2 Reduction Catalyzed by Tricarbonyl Rhenium(I) Complexes with Diimine Ligands: Strikingly Slow Formation of the Re−Re and Re−C(O)O−Re Species from Re(dmb)$(CO)_3$S (dmb = 4,4‘-Dimethyl-2,2‘-bipyridine, S = Solvent). *J. Am. Chem. Soc.* **2003**, *125* (39), 11976-11987. DOI: 10.1021/ja035960a.

(18) Chattopadhyay, S.; Cheah, M. H.; Lomoth, R.; Hammarström, L. Direct Detection of Key Intermediates during the Product Release in Rhenium Bipyridine-Catalyzed CO_2 Reduction Reaction. *ACS Catal.* **2024**, *14* (21), 16324-16334. DOI: 10.1021/acscatal.4c06044.

(19) Bhattacharyya, K.; Das, P. Nanosecond transient processes in the triethylamine quenching of benzophenone triplets in aqueous alkaline media. Substituent effect, ketyl radical deprotonation, and secondary photoreduction kinetics. *J. Phys. Chem. A* **1986**, *90* (17), 3987-3993.

(20) Kutal, C.; Corbin, A. J.; Ferraudi, G. Further studies of the photoinduced reduction of carbon dioxide mediated by tricarbonylbromo (2, 2'-bipyridine) rhenium (I). *Organometallics* **1987**, *6* (3), 553-557.

(21) Balzani, V.; Piotrowiak, P.; Rodgers, M.; Mattay, J.; Astruc, D. *Electron transfer in chemistry*; Wiley-VCh Weinheim, 2001. DOI: 10.1002/9783527618248.

(22) Wayner, D. D.; McPhee, D.; Griller, D. Oxidation and reduction potentials of transient free radicals. *J. Am. Chem. Soc.* **1988**, *110* (1), 132-137.

(23) Carr, C. R.; Vrionides, M. A.; Grills, D. C. Reactivity of radiolytically and photochemically generated tertiary amine radicals towards a CO_2 reduction catalyst. *J. Chem. Phys.* **2023**, *159* (24), 244503. DOI: 10.1063/5.0180065.

(24) Ho, P.-Y.; Cheng, S.-C.; Yu, F.; Yeung, Y.-Y.; Ni, W.-X.; Ko, C.-C.; Leung, C.-F.; Lau, T.-C.; Robert, M. Light-Driven Reduction of CO_2 to CO in Water with a Cobalt Molecular Catalyst and an Organic Sensitizer. *ACS Catal.* **2023**, *13* (9), 5979-5985. DOI: 10.1021/acscatal.3c00036.

(25) Navalón, S.; Dhakshinamoorthy, A.; Álvaro, M.; Ferrer, B.; García, H. Metal–Organic Frameworks as Photocatalysts for Solar-Driven Overall Water Splitting. *Chem. Rev.* **2023**, *123* (1), 445-490. DOI: 10.1021/acs.chemrev.2c00460.

(26) Kinoshita, Y.; Deromachi, N.; Kajiwara, T.; Koizumi, T.-a.; Kitagawa, S.; Tamiaki, H.; Tanaka, K. Photoinduced Catalytic Organic-Hydride Transfer to CO_2 Mediated with Ruthenium Complexes as NAD^+/NADH Redox Couple Models. *ChemSusChem* **2023**, *16* (6), e202300032. DOI: 10.1002/cssc.202300032.

(27) Xie, Z.-L.; Gupta, N.; Niklas, J.; Poluektov, O. G.; Lynch, V. M.; Glusac, K. D.; Mulfort, K. L. Photochemical charge accumulation in a heteroleptic copper(I)-anthraquinone molecular dyad via proton-coupled electron transfer. *Chem. Sci.* **2023**, *14* (37), 10219-10235. DOI: 10.1039/D3SC03428C

(28) Su, C.; Chen, Z.; Feng, Q.; Wei, F.; Mo, A.; Huang, H.-H.; Hu, H.; Zou, H.; Liang, F.; Liu, D. Electronic effects promoted the catalytic activities of binuclear Co(II) complexes for visible-light-driven CO_2 reduction in a water-containing system. *Dalton Trans.* **2023**, *52* (14), 4548-4553. DOI: 10.1039/D3DT00054K.

(29) Bruschi, C.; Gui, X.; Rauthe, P.; Fuhr, O.; Unterreiner, A.-N.; Klopper, W.; Bizzarri, C. Dual Role of a Novel Heteroleptic Cu(I) Complex in Visible-Light-Driven CO_2 Reduction. *Chem. Eur. J.* **2024**, *30* (44), e202400765. DOI: 10.1002/chem.202400765.

(30) Beil, S. B.; Bonnet, S.; Casadevall, C.; Detz, R. J.; Eisenreich, F.; Glover, S. D.; Kerzig, C.; Næsborg, L.; Pullen, S.; Storch, G.; et al. Challenges and Future Perspectives in Photocatalysis: Conclusions from an Interdisciplinary Workshop. *JACS Au* **2024**, *4* (8), 2746-2766. DOI: 10.1021/jacsau.4c00527.

(31) Grills, D. C.; Farrington, J. A.; Layne, B. H.; Lymar, S. V.; Mello, B. A.; Preses, J. M.; Wishart, J. F. Mechanism of the formation of a Mn-based CO2 reduction catalyst revealed by pulse radiolysis with time-resolved infrared detection. *J. Am. Chem. Soc.* **2014**, *136* (15), 5563-5566.

(32) Clark, M. L.; Cheung, P. L.; Lessio, M.; Carter, E. A.; Kubiak, C. P. Kinetic and Mechanistic Effects of Bipyridine (bpy) Substituent, Labile Ligand, and Brønsted Acid on Electrocatalytic CO_2 Reduction by Re(bpy) Complexes. *ACS Catal.* **2018**, *8* (3), 2021-2029. DOI: 10.1021/acscatal.7b03971.

(33) Müller, A. V.; Wierzba, W. M.; do Nascimento, L. G. A.; Concepcion, J. J.; Nikolaou, S.; Polyansky, D. E.; Polo, A. S. Tuning the Photocatalytic CO2 Reduction through para-Substituents in Bipyridyl Rhenium Complexes. *Artificial Photosynthesis* **2025**. DOI: 10.1021/aps.4c00026.

(34) Espinosa, M. R.; Ertem, M. Z.; Barakat, M.; Bruch, Q. J.; Deziel, A. P.; Elsby, M. R.; Hasanayn, F.; Hazari, N.; Miller, A. J. M.; Pecoraro, M. V.; et al. Correlating Thermodynamic and Kinetic Hydricities of Rhenium Hydrides. *J. Am. Chem. Soc.* **2022**, *144* (39), 17939-17954. DOI: 10.1021/jacs.2c07192.

(35) Elgrishi, N.; Rountree, K. J.; McCarthy, B. D.; Rountree, E. S.; Eisenhart, T. T.; Dempsey, J. L. A Practical Beginner’s Guide to Cyclic Voltammetry. *J. Chem. Educ.* **2018**, *95* (2), 197-206. DOI: 10.1021/acs.jchemed.7b00361.

(36) Valencia, D. P.; González, F. J. Understanding the linear correlation between diffusion coefficient and molecular weight. A model to estimate diffusion coefficients in acetonitrile solutions. *Electrochem. Commun.* **2011**, *13* (2), 129-132. DOI: 10.1016/j.elecom.2010.11.032.

(37) Hansch, C.; Leo, A.; Taft, R. A survey of Hammett substituent constants and resonance and field parameters. *Chem. Rev.* **1991**, *91* (2), 165-195.

(38) Wishart, J. F.; Cook, A. R.; Miller, J. R. The LEAF picosecond pulse radiolysis facility at Brookhaven National Laboratory. *Rev. Sci. Instrum.* **2004**, *75* (11), 4359-4366. DOI: 10.1063/1.1807004.

(39) Polyansky, D. E.; Manbeck, G. F.; Ertem, M. Z. Combined Effects of Hemicolligation and Ion Pairing on Reduction Potentials of Biphenyl Radical Cations. *J. Phys. Chem. A* **2023**, *127* (38), 7918-7927. DOI: 10.1021/acs.jpca.3c03817.

(40) Bird, M. J.; Iyoda, T.; Bonura, N.; Bakalis, J.; Ledbetter, A. J.; Miller, J. R. Effects of electrolytes on redox potentials through ion

pairing. *J. Electroanal. Chem.* **2017**, *804*, 107-115. DOI: 10.1016/j.jelechem.2017.09.030.

(41) Bird, M. J.; Pearson, M. A.; Asaoka, S.; Miller, J. R. General Method for Determining Redox Potentials without Electrolyte. *J. Phys. Chem. A* **2020**, *124* (26), 5487-5495. DOI: 10.1021/acs.jpca.0c02948.

(42) Grills, D. C.; Lymar, S. V. Solvated Electron in Acetonitrile: Radiation Yield, Absorption Spectrum, and Equilibrium between Cavity- and Solvent-Localized States. *J. Phys. Chem. B* **2022**, *126* (1), 262-269. DOI: 10.1021/acs.jpcb.1c08946.

(43) Grills, D. C.; Lymar, S. V. Radiolytic formation of the carbon dioxide radical anion in acetonitrile revealed by transient IR spectroscopy. *PCCP* **2018**, *20* (15), 10011-10017, 10.1039/C8CP00977E. DOI: 10.1039/C8CP00977E.

(44) Samant, V.; Singh, A. K.; Mukherjee, T.; Palit, D. K. Spectroscopic properties of anion radicals studied using pulse radiolysis. *Res. Chem. Intermed.* **2006**, *32*, 767-776. DOI: 10.1163/156856706778606499.

(45) John, R. M.; Matthew, J. B. Effects of Electrolyte on Redox Potentials. In *Redox Chemistry*, Olivier, F. Ed.; IntechOpen, 2022; p Ch. 4.

(46) Savéant, J.-M. Single Electron Transfer at an Electrode. In *Elements of Molecular and Biomolecular Electrochemistry*, 2006; pp 1-77.

(47) Goez, M.; Sartorius, I. Photo-CIDNP investigation of the deprotonation of aminium cations. *J. Am. Chem. Soc.* **1993**, *115* (24), 11123-11133. DOI: 10.1021/ja00077a009.

(48) McLauchlan, K. A.; Ritchie, A. J. D. Spin-polarized (CIDEP) neutral α-aminoalkyl radicals from tertiary amines observed in solution by flash-photolysis electron spin resonance. *J. Chem. Soc. Perkin Trans. 2* **1984**, (2), 275-279, 10.1039/P29840000275. DOI: 10.1039/P29840000275.

(49) Misik, V.; Riesz, P. Free Radical Formation by Ultrasound in Organic Liquids: A Spin Trapping and EPR Study. *J. Phys. Chem.* **1994**, *98* (6), 1634-1640. DOI: 10.1021/j100057a016.

(50) Takeda, N.; Miller, J. R. Inverted Region in Bimolecular Electron Transfer in Solution Enabled by Delocalization. *J. Am. Chem. Soc.* **2020**, *142* (42), 17997-18004. DOI: 10.1021/jacs.0c04780.

(51) Burshtein, A. I.; Georgievski, Y. Energy activation of adiabatic and nonadiabatic electron transfer. *J. Chem. Phys.* **1994**, *100* (10), 7319-7330. DOI: 10.1063/1.466876.

(52) Myong, M. S.; Bird, M. J.; Miller, J. R. Kinetics and Energetics of Electron Transfer to Dimer Radical Cations. *J. Phys. Chem. A* **2023**, *127* (13), 2881-2886. DOI: 10.1021/acs.jpcb.2c07302.

(53) Cook, A. R. Sub-picosecond Production of Solute Radical Cations in Tetrahydrofuran after Radiolysis. *J. Phys. Chem. A* **2021**, *125* (47), 10189-10197. DOI: 10.1021/acs.jpca.1c08568.

(54) Zhao, Y.; Truhlar, D. G. The M06 suite of density functionals for main group thermochemistry, thermochemical kinetics, noncovalent interactions, excited states, and transition elements: two new functionals and systematic testing of four M06-class functionals and 12 other functionals. *Theor. Chem. Acc.* **2008**, *120* (1), 215-241. DOI: 10.1007/s00214-007-0310-x.

(55) Cossi, M.; Barone, V.; Mennucci, B.; Tomasi, J. Ab initio study of ionic solutions by a polarizable continuum dielectric model. *Chem. Phys. Lett.* **1998**, *286* (3), 253-260. DOI: 10.1016/S0009-2614(98)00106-7.

(56) Grimme, S.; Hansen, A.; Ehlert, S.; Mewes, J.-M. r2SCAN-3c: A "Swiss army knife" composite electronic-structure method. *J. Chem. Phys.* **2021**, *154* (6), 064103. DOI: 10.1063/5.0040021.

(57) Bannwarth, C.; Ehlert, S.; Grimme, S. GFN2-xTB—An Accurate and Broadly Parametrized Self-Consistent Tight-Binding Quantum Chemical Method with Multipole Electrostatics and Density-Dependent Dispersion Contributions. *J. Chem. Theory Comput.* **2019**, *15* (3), 1652-1671. DOI: 10.1021/acs.jctc.8b01176.

(58) Eriksen, J.; Foote, C. S. Electron-transfer fluorescence quenching and exciplexes of cyano-substituted anthracenes. *J. Phys. Chem. A* **1978**, *82* (25), 2659-2662.

(59) Kosugi, K.; Kondo, M.; Masaoka, S. Quick and easy method to dramatically improve the electrochemical CO_2 reduction activity of an iron porphyrin complex. *Angew. Chem., Int. Ed.* **2021**, *60* (40), 22070-22074.

(60) Stratakes, B. M.; Wells, K. A.; Kurtz, D. A.; Castellano, F. N.; Miller, A. J. M. Photochemical H_2 Evolution from Bis(diphosphine)nickel Hydrides Enables Low-Overpotential Electrocatalysis. *J. Am. Chem. Soc.* **2021**, *143* (50), 21388-21401. DOI: 10.1021/jacs.1c10628.

TOC